





RESEARCH ARTICLE | JUNE 23 2025

Slip correction and transient treatment of pressure oscillation method for permeability measurement

Mingbao Zhang  ; Zhiguo Tian  ; Moran Wang  



Rev. Sci. Instrum. 96, 063904 (2025)

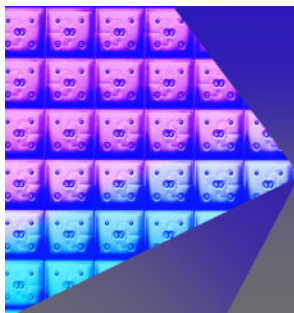
<https://doi.org/10.1063/5.0196658>



Articles You May Be Interested In

Two-scale structure of the current layer controlled by meandering motion during steady-state collisionless driven reconnection

Phys. Plasmas (July 2004)



Review of
Scientific Instruments
Special Topics Now Online

[Learn More](#)



Slip correction and transient treatment of pressure oscillation method for permeability measurement

Cite as: Rev. Sci. Instrum. 96, 063904 (2025); doi: 10.1063/5.0196658

Submitted: 8 January 2024 • Accepted: 25 May 2025 •

Published Online: 23 June 2025



View Online



Export Citation



CrossMark

Mingbao Zhang,  Zhiguo Tian,  and Moran Wang^{a)} 

AFFILIATIONS

Department of Engineering Mechanics, Tsinghua University, Beijing 100084, China

^{a)} Author to whom correspondence should be addressed: mrwang@tsinghua.edu.cn

ABSTRACT

The pressure oscillation method is a technique for measuring the permeability of evolving porous media. This study presents the analytical solution of the pressure oscillation process considering the slip boundary based on the capillary model and perturbation expansion. The correspondence between the Klinkenberg relation and the Knudsen number is clarified, which provides a theoretical basis for applying the Klinkenberg correction to the pressure oscillation method. The data treatment method using the transient term is proposed, along with its applicable range. Experiments of the pressure oscillation method and pulse decay method are carried out to validate the method. The results show that the transient solution is consistent with the periodic solution, and the unification of the quasi-steady-state and unsteady-state methods under pressure oscillation conditions is achieved. In terms of measurement duration, the pressure oscillation method reduces the measurement time by at least four times compared to the classical pulse decay method. Based on the solution of permeability and porosity, the parameter effects on the experimental data are analyzed, and the dimensionless phase diagram of the amplitude ratio is given to provide a reference for practical engineering applications.

Published under an exclusive license by AIP Publishing. <https://doi.org/10.1063/5.0196658>

I. INTRODUCTION

Permeability is one of the most important parameters to characterize the ability of fluid flow through a porous medium (Hadia *et al.*, 2012; Tian *et al.*, 2023). The conventional permeability measurements usually focus on fixed structures, while the evolution of time-dependent porous media requires continuous measurements (Gong *et al.*, 2023; Liu *et al.*, 2021), such as processes like rock creep (An *et al.*, 2021) and nuclear waste disposal (Abe *et al.*, 2022; Ohazuruike and Lee, 2023). The classical permeability measurement methods mainly consist of steady-state and unsteady-state methods (Sander *et al.*, 2017; Wang *et al.*, 2021). The steady-state method, derived from Darcy's law (Darcy, 1856), calculates permeability by recording the flow rates at a given pressure difference (Cheng *et al.*, 2008; Fellah *et al.*, 2007; Liu *et al.*, 2006; Wyckoff *et al.*, 1933). However, this method requires a long equilibration time when measuring low-permeability porous media, and the measurement error becomes significant at low flow rates (Green *et al.*, 1999; Malkovsky *et al.*, 2009). The unsteady-state method mainly includes

the pulse-decay method (Brace *et al.*, 1968), the Gas Research Institute (GRI) method (Jannot *et al.*, 2021; Luffel and Guidry, 1992), and the pressure oscillation method (Bernabé *et al.*, 2006; Kranz *et al.*, 1990), among others. The pulse decay method applies one or multiple pulses [called the Step Decay method (Lasseux *et al.*, 2012)] to calculate permeability using historical matching (Jannot *et al.*, 2008) and straight-line methods, enabling rapid and high-precision measurement of permeability (Wang *et al.*, 2022). However, it cannot achieve continuous measurements as it requires pressure equilibrium before each measurement (Boulin *et al.*, 2012). In addition, both the steady-state method and the pulse decay method are influenced by the effective stress difference and are sensitive to environmental factors such as leaks and temperature fluctuations, as well as changes in internal parameters (Jones and Meredith, 1998; Sander *et al.*, 2017).

The pressure oscillation method compensates for the weakness of the pulse decay method, enabling continuous measurements (Hasanov *et al.*, 2020; Lebedev *et al.*, 2018; Uehara and Shimamoto, 2004). Utilizing relative values over multiple periods for

permeability calculations, this method exhibits insensitivity to external parameter variations while maintaining the average effective stress constant (Kranz *et al.*, 1990). Initially employed for measuring the thermal diffusivity of materials, Kranz *et al.* (1990) and Fischer (1992) later extended this technique to measure the permeability and storage capacity. The experimental apparatus for the pressure oscillation method consists mainly of upstream and downstream chambers along with a sample holder. A pressure oscillation (e.g., sinusoidal wave) is applied to the upstream chamber, controlled by a function generator regulating the pressure pump or fluid discharge (Pamuk and Özdemir, 2012). Due to damping effects from the porous medium, the oscillation detected in the downstream chamber exhibits amplitude decay and phase changes, which can be used to calculate the permeability (Winhausen *et al.*, 2020). By incorporating diffusion equations based on mass conservation with oscillation boundary conditions, the analytical solution is derived and can be separated into periodic and transient parts, so the method is considered to be between the steady state and unsteady state (Fischer, 1992). However, current experiments exclusively utilize the periodic part for the permeability calculation, representing phase difference and amplitude ratio as functions of two dimensionless numbers. Employing a nomograph, the permeability and storage capacity are inversely determined from these dimensionless numbers (Bernabé *et al.*, 2006; Winhausen *et al.*, 2020). The utilization of the transient part in the analytical solution awaits further development. In addition, the challenges in the application of the pressure oscillation method involve the setting of appropriate parameters such as period and downstream chamber volume. The trial-and-error process of experimental parameter optimization is likely to increase both the time and equipment costs. Furthermore, inappropriate setup of experimental parameters can lead to deviations in the results (Assady *et al.*, 2019; Jin *et al.*, 2015; Winhausen *et al.*, 2020). Developing reasonable prognostic setup conditions to reduce the cost of trial and error is necessary.

In tight porous materials with pores at the micro–nano level, the gas measurement process is susceptible to the slip effect. In experiments reported by previous authors, the pressure oscillation method agrees with the steady-state method in high-permeability sandstones, while there is a gap in low-permeability samples (Song and Renner, 2006). In measurements consistent with both the pulse decay method and the steady-state method, the pressure oscillation method yielded significantly higher results, which is thought to be possibly caused by erroneous frequencies or downstream pressure fluctuations (Assady *et al.*, 2019). The difference between permeability measured with argon and water in the same medium was attributed to physical–chemical interactions between fault clay and water (Faulkner and Rutter, 2000). These discrepancies may be attributed to errors induced by the slip effect. The classical correction method for the slip effect is the Klinkenberg correction, which involves measuring and calculating the apparent permeability at multiple average effective pressures and obtaining the intrinsic permeability from the intercept through linear fitting (Jannot and Lasseux, 2012). The upscaling of slip correction from pore-scale to macro-scale has been achieved by methods such as volume averaging (Lasseux *et al.*, 2014; Lasseux *et al.*, 2019; Lasseux *et al.*, 2016; Skjetne and Auriault, 1999). In the process of the pressure oscillation experiment, the Klinkenberg correction also has been applied to correct the results of low-permeability samples, yielding results consistent

with steady-state methods (Knabe and Wang, 2011). However, the Klinkenberg correction is derived based on steady-state flow and lacks theoretical support for its application in the pressure oscillation method. The approach adopted by Kranz *et al.* (1990) originates from the apparent diffusion equation and does not allow for the direct introduction of slip boundaries. Moreover, obtaining an analytical solution by substituting the Klinkenberg equation into the diffusion equation is also difficult.

Synthesizing the previous research, the theoretical foundation, the utilization of the transient solution, and the method for regulating parameters in the pressure oscillation method remain to be developed. In light of the aforementioned issues and objectives, this work is organized into the following sections: In Sec. II, the analytical solution introducing the slip boundary condition in the pressure oscillation method is derived based on the capillary model and perturbation expansion, offering a microscopic explanation for the slip effect in measurements. In Sec. III, the correspondence between the slip effect and the Klinkenberg correction is given, providing a theoretical basis for the utilization of the Klinkenberg correction. A new data processing method is proposed for permeability calculation based on the transient solution, and the scope of application of the Klinkenberg correction for the new method is given. In Sec. IV, the experiments of the pressure oscillation method and pulse decay method are conducted to validate the theoretical model and data processing method, respectively, and the permeability measurement results and measurement time are compared. The parameter regulation method according to the calculation process is presented to provide a reference for the practical application in production. Finally, conclusions are presented in Sec. V.

II. PHYSICAL AND MATHEMATICAL MODEL

A. Governing equation and perturbation expansion

The capillary model approximates the porous medium as a straight channel formed by a cluster of tube bundles, which describes the equivalent flow relationship with the porous medium, as shown in Fig. 1. Based on the equal flow rate between the macroscopic Darcy's law for porous media and the circular Poiseuille flow driven by pressure difference, the relationship between permeability, porosity, and radius of the approximated circular tube can be established by the following equation:

$$k = \frac{\phi R^2}{8}, \quad (1)$$

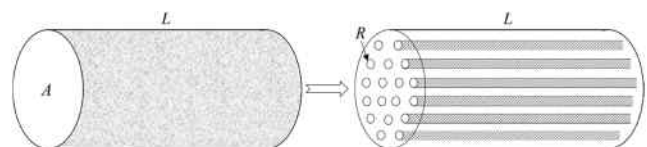


FIG. 1. Schematic of the capillary model. The porous medium is approximated as a straight channel formed by a cluster of tube bundles. A and L are the cross-sectional area and length of a porous medium, respectively. R is the radius of the circular tube in the capillary model.

where k (m^2) is the permeability, ϕ is the porosity, and R (m) is the radius of the circular tube in the capillary model. This model transforms the solving of the macroscopic diffusion equations into the solving of the equations for circular tube flow. Klinkenberg used this model in combination with the slip boundary condition to derive the corrected permeability in the steady state, which reveals the microscopic mechanism of the slip effect. The general Klinkenberg formula can be expressed as

$$k_{app} = k_{int} \left(1 + \frac{b}{\bar{P}} \right), \quad (2)$$

where k_{app} (m^2) is the apparent permeability, k_{int} (m^2) is the intrinsic permeability, \bar{P} (Pa) is the mean pore pressure, and b is the correction factor. This formula is widely used for the calculation of intrinsic permeability corrected for the slip effect.

This study employs the capillary tube model to simplify the representation of a porous medium, allowing the internal flow to be considered as a single-tube flow. Correspondingly, for gas flow in capillaries, the compressible Navier–Stokes equations can be expressed as

$$\rho \frac{\partial u}{\partial t} + \rho u \frac{\partial u}{\partial z} = \mu \left(\frac{\partial^2 u}{\partial r^2} + \frac{1}{r} \frac{\partial u}{\partial r} + \frac{\partial^2 u}{\partial z^2} \right) - \frac{\partial P}{\partial z}, \quad (3)$$

where ρ (kg m^{-3}) is the fluid density, μ (Pa s) is the dynamic viscosity, r (m) is the radial coordinate, z (m) is the flow coordinate, u (m s^{-1}) is the flow velocity, P (Pa) is the pressure, and t (s) is the time. The above equation is inherently difficult to solve, and extensive previous work on the equation has demonstrated that when the radius of the circular tube is much smaller than the flow length $R \ll L$, the mean density $\bar{\rho} = \frac{\rho_u + \rho_d}{2}$ can be used for calculating the mass flow rate, $Q_m = \frac{\pi(P_u - P_d)R^4 \bar{\rho}}{8 \mu L}$, where P_u (Pa) and P_d (Pa) represent the pressure at the upstream inlet and the downstream outlet, respectively. ρ_u (kg m^{-3}) and ρ_d (kg m^{-3}) represent the density at the upstream inlet and the downstream outlet, respectively (Veltzke and Thöming, 2012; Wang et al., 2018). In the capillary model, the condition that the radius R is much smaller than the length L is evidently satisfied. Given that the primary characteristic of flow in porous media is mass flux, the governing equations can be expressed using the incompressible Navier–Stokes (NS) equations represented with average density. The case of small amplitude pressure oscillation is considered where the oscillation pressure is less than 10% of the equilibrium pressure, so the convective term can be neglected. In addition, the small variations in density and viscosity due to pressure oscillations indicate that using average values is reasonable. The simplified incompressible NS equation is

$$\frac{\partial u}{\partial t} = \bar{\nu} \frac{\partial^2 u}{\partial z^2} + \bar{\nu} \left(\frac{\partial^2 u}{\partial r^2} + \frac{1}{r} \frac{\partial u}{\partial r} \right) - \frac{1}{\bar{\rho}} \frac{\partial P}{\partial z}, \quad (4)$$

where $\bar{\rho}$ (kg m^{-3}) and $\bar{\nu}$ ($\text{m}^2 \text{s}^{-1}$) represent the average density and average dynamic viscosity of the fluid, respectively.

The magnitude analysis of the equation terms can clarify the corresponding relationships between these terms. The viscous force and pressure-driven force of all fluid flow through the tubes should be of the same order of magnitude. That is $\frac{\bar{\mu}}{R} \cdot N \cdot \pi RL$ and $\Delta P(t) \cdot$

$N\pi R^2$ should have the same order of magnitude, where \bar{u} is the average velocity, $\bar{\mu}$ is the average dynamic viscosity, N is the number of tubes in the capillary model, and $\Delta P(t)$ is the pressure difference between upstream and downstream at the time t . Simplifying this relationship yields the mean velocity $\bar{u} \approx \frac{\Delta P(t)R^2}{\bar{\mu}L}$, which has the same order of magnitude as the average velocity in laminar flow driven by pressure in a cylindrical tube. Subsequently, the following dimensionless quantities are introduced for nondimensionalizing the above Eq. (4):

$$\tilde{z} = \frac{z}{L}, \tilde{r} = \frac{r}{R}, \tilde{u} = \frac{u}{\bar{u}}, \tilde{P} = \frac{P(t)}{P_A}, \tilde{t} = \frac{t}{t_c} = \frac{R^2 P_0}{8\bar{\mu}L^2} t, \quad (5)$$

where quantities with a tilde (\sim) are dimensionless. P_A (Pa) represents the pressure amplitude of the upstream, P_0 (Pa) is the initial equilibrium pressure, and the characteristic time is taken as $t_c = \frac{8\bar{\mu}L^2}{R^2 P_0}$ (s). Consequently, the dimensionless form of the incompressible NS equations is

$$\frac{R^4 P_0}{8\bar{\mu}\bar{\nu}L^2} \frac{\partial \tilde{u}}{\partial \tilde{t}} = \frac{R^2}{L^2} \frac{\partial^2 \tilde{u}}{\partial \tilde{z}^2} + \frac{\partial^2 \tilde{u}}{\partial \tilde{r}^2} + \frac{1}{\tilde{r}} \frac{\partial \tilde{u}}{\partial \tilde{r}} - \frac{R^2 P_A}{\bar{\mu}\bar{u}L} \frac{\partial \tilde{P}}{\partial \tilde{z}}. \quad (6)$$

Substituting the mean velocity \bar{u} into Eq. (6) for a magnitude analysis, the order of magnitude of $\frac{\partial \tilde{P}}{\partial \tilde{z}}$ is given by $\frac{R^2 P_A}{\bar{\mu}\bar{u}L} \approx \frac{P_A}{\Delta P(t)} \approx 1$. In a realistic physical process of pressure oscillations, the transient term induces variations in velocity in the flow direction, yielding $\frac{R^4 P_0}{8\bar{\mu}\bar{\nu}L^2} \approx \frac{R^2}{L^2}$. Combining the magnitude analysis above, it follows that $\frac{P_A}{P_0} \approx \frac{\bar{u}L}{8\bar{\nu}}$. Since the experimental requirements dictate that the amplitude of pressure oscillations is much smaller than the equilibrium pressure, avoiding changes in pore elasticity and fluid compressibility caused by pressure fluctuations, it is reasonable to assume $\frac{P_A}{P_0} \ll 1$. Accordingly, $\frac{\bar{u}L}{\bar{\nu}}$, which is the expression for the Reynolds number, is also much less than 1, consistent with the small pressure difference. In addition, simplifying $\frac{R^4 P_0}{8\bar{\mu}\bar{\nu}L^2} \approx \frac{R^2}{L^2}$ to $R^2 \approx \frac{8\bar{\mu}\bar{\nu}}{P_0}$ and substituting it into the expression for the characteristic time yields $t_c = \frac{L^2}{\bar{\nu}}$, indicating that the characteristic time represents the momentum diffusion of the fluid in the flow direction.

In the capillary model assumption, the radius R of the circular tube is significantly smaller than its length L . Therefore, the ratio of the two, $\varepsilon = \frac{R}{L}$, can be employed as a small quantity for perturbation expansion. By incorporating the small quantity ε through the magnitude analysis into the governing equation, Eq. (6) can be further simplified as

$$\varepsilon^2 \frac{\partial \tilde{u}}{\partial \tilde{t}} = \varepsilon^2 \frac{\partial^2 \tilde{u}}{\partial \tilde{z}^2} + \frac{\partial^2 \tilde{u}}{\partial \tilde{r}^2} + \frac{1}{\tilde{r}} \frac{\partial \tilde{u}}{\partial \tilde{r}} - \frac{\partial \tilde{P}}{\partial \tilde{z}}. \quad (7)$$

The perturbation expansion of velocity and pressure using the small quantity ε can be obtained,

$$\tilde{u} = \tilde{u}^{(0)} + \varepsilon \tilde{u}^{(1)} + \varepsilon^2 \tilde{u}^{(2)} + \dots, \quad (8)$$

$$\tilde{P} = \tilde{P}^{(0)} + \varepsilon \tilde{P}^{(1)} + \varepsilon^2 \tilde{P}^{(2)} + \dots. \quad (9)$$

As the parameter ε approaches zero, Eqs. (8) and (9) tend to approximate \tilde{u}, \tilde{P} , respectively, but increasing the number of terms cannot

be relied upon to improve the accuracy of the approximation. Substituting Eqs. (8) and (9) into Eq. (7) yields

$$\mathcal{O}(1) : \frac{\partial^2 \tilde{u}^{(0)}}{\partial \tilde{r}^2} + \frac{1}{\tilde{r}} \frac{\partial \tilde{u}^{(0)}}{\partial \tilde{r}} - \frac{\partial \tilde{P}^{(0)}}{\partial \tilde{z}} = 0, \quad (10a)$$

$$\mathcal{O}(\varepsilon) : \frac{\partial^2 \tilde{u}^{(1)}}{\partial \tilde{r}^2} + \frac{1}{\tilde{r}} \frac{\partial \tilde{u}^{(1)}}{\partial \tilde{r}} - \frac{\partial \tilde{P}^{(1)}}{\partial \tilde{z}} = 0, \quad (10b)$$

$$\mathcal{O}(\varepsilon^2) : \frac{\partial \tilde{u}^{(0)}}{\partial \tilde{t}} = \frac{\partial^2 \tilde{u}^{(0)}}{\partial \tilde{z}^2} + \left(\frac{\partial^2 \tilde{u}^{(2)}}{\partial \tilde{r}^2} + \frac{1}{\tilde{r}} \frac{\partial \tilde{u}^{(2)}}{\partial \tilde{r}} \right) - \frac{\partial \tilde{P}^{(2)}}{\partial \tilde{z}}, \quad (10c)$$

where $\mathcal{O}(1)$ indicates that each term in the equation is of magnitude 1, and similarly, $\mathcal{O}(\varepsilon)$ and $\mathcal{O}(\varepsilon^2)$ follow the same logic. Combining Eqs. (10a) and (10b), the equation $\frac{\partial^2}{\partial \tilde{r}^2} [\tilde{u}^{(0)} + \varepsilon \tilde{u}^{(1)}] + \frac{1}{\tilde{r}} \frac{\partial}{\partial \tilde{r}} [\tilde{u}^{(0)} + \varepsilon \tilde{u}^{(1)}] - \frac{\partial}{\partial \tilde{z}} [\tilde{P}^{(0)} + \varepsilon \tilde{P}^{(1)}] = 0$ can be obtained.

Therefore, it is reasonable to assume that $\frac{\partial^2 \tilde{u}}{\partial \tilde{r}^2} + \frac{1}{\tilde{r}} \frac{\partial \tilde{u}}{\partial \tilde{r}} - \frac{\partial \tilde{P}}{\partial \tilde{z}} = 0$ holds if only the first two terms of the perturbation expansion approximate Eqs. (8) and (9) for pressure and velocity. Furthermore, by utilizing the first three terms of the perturbation expansion to approximate the pressure and velocity in Eqs. (8) and (9) and, subsequently, substituting them into equation $\frac{\partial^2 \tilde{u}}{\partial \tilde{r}^2} + \frac{1}{\tilde{r}} \frac{\partial \tilde{u}}{\partial \tilde{r}} - \frac{\partial \tilde{P}}{\partial \tilde{z}} = 0$, the following equation can be derived: $\frac{\partial^2 \tilde{u}^{(2)}}{\partial \tilde{r}^2} + \frac{1}{\tilde{r}} \frac{\partial \tilde{u}^{(2)}}{\partial \tilde{r}} - \frac{\partial \tilde{P}^{(2)}}{\partial \tilde{z}} = 0$. Substituting this formula into Eq. (10c), the governing equations at different orders can be expressed as

$$\frac{\partial^2 \tilde{u}^{(0)}}{\partial \tilde{r}^2} + \frac{1}{\tilde{r}} \frac{\partial \tilde{u}^{(0)}}{\partial \tilde{r}} - \frac{\partial \tilde{P}^{(0)}}{\partial \tilde{z}} = 0, \quad (11)$$

$$\frac{\partial \tilde{u}^{(0)}}{\partial \tilde{t}} = \frac{\partial^2 \tilde{u}^{(0)}}{\partial \tilde{z}^2}. \quad (12)$$

Equation (11) describes the pressure-driven flow inside the circular tube, considering only radial variations in velocity. Equation (12) characterizes the axial changes in fluid flow within the tube due to the influence of transient terms. These two equations can be solved separately.

B. Boundary condition and analytical solution

Based on the above analysis, Eq. (11) can be solved directly. Consider the boundary conditions,

$$\tilde{u}^{(0)} \Big|_{\tilde{r}=0} \neq \infty, \quad (13)$$

$$\tilde{u}^{(0)} \Big|_{\tilde{r}=1} = -\frac{2 - \sigma_u}{\sigma_u} Kn \frac{\partial \tilde{u}^{(0)}}{\partial \tilde{r}} \Big|_{\tilde{r}=1}, \quad (14)$$

where the Knudsen number $Kn = \frac{\lambda}{R}$ characterizing the slip effect is calculated by the ratio of the molecule mean free path λ to the radius of the circular tube R . The molecular mean free path λ is a function of the reciprocal of pressure. Given that the amplitude of pressure does not exceed 10% of the equilibrium pressure, the molecular mean free path fluctuates only between 0.9 and 1.1 times the value corresponding to the equilibrium pressure. Furthermore, since the

pressure oscillations are periodic, this study reasonably assumes that the molecular mean free path and the Kn number over multiple cycles are solely dependent on the equilibrium pressure. σ_u is the accommodation coefficient, which depends on the specific gas and the surface quality. The condition of full diffusive reflection is considered, with $\sigma_u = 1$ and $\frac{2 - \sigma_u}{\sigma_u} = 1$, so the accommodation coefficient is omitted in the subsequent text. Equation (13) indicates that the velocity at the center of the circular tube cannot be infinitely large, and Eq. (14) represents the slip boundary condition. By combining these two boundary conditions, Eq. (11) can be directly solved,

$$\tilde{u}^{(0)} = -\frac{1}{4} \frac{\partial \tilde{P}^{(0)}}{\partial \tilde{z}} (1 - \tilde{r}^2 + 2Kn). \quad (15)$$

Taking the cross-sectional average of Eq. (15), the average velocity can be expressed as

$$\overline{\tilde{u}^{(0)}} = \frac{\int_0^R \tilde{u}^{(0)} \cdot 2\pi r dr}{\pi R^2} = -\frac{1}{8} \frac{\partial \tilde{P}^{(0)}}{\partial \tilde{z}} (1 + 4Kn). \quad (16)$$

As the pressure oscillation method focuses on pressure variations, Eq. (12) needs to be transformed into an equation related to pressure. Averaging along the radial direction, similar to the form of Eqs. (12) and (16), can be transformed into the derivative of pressure with respect to \tilde{t} and \tilde{z} due to the fact that the orders of derivatives and integrals can be switched in fluid mechanics, $\frac{\partial}{\partial \tilde{z}} \left(\frac{\partial \tilde{P}^{(0)}}{\partial \tilde{t}} \right) = \frac{\partial}{\partial \tilde{z}} \left(\frac{\partial^2 \tilde{P}^{(0)}}{\partial \tilde{z}^2} \right)$. Without considering the integration in the axial direction, the following diffusion equation is necessarily a solution of that equation:

$$\frac{\partial \tilde{P}^{(0)}}{\partial \tilde{t}} = \frac{\partial^2 \tilde{P}^{(0)}}{\partial \tilde{z}^2}. \quad (17)$$

The solution of Eq. (17) requires incorporating the upstream and downstream boundary conditions from the pressure oscillation process. As depicted in Fig. 2, for the upstream inlet, a stable sinusoidal pressure change is provided using cyclic compression or exhaust, $P_u(t) = P_A \sin(\omega t + \delta) + P_0$, where ω is the angular velocity of amplitude change and δ is the initial phase. Therefore, the upstream can be characterized by the first type of dimensionless boundary condition,

$$\tilde{P} \Big|_{\tilde{z}=1} = \sin(\omega \tilde{t} + \delta) + \beta, \quad (18)$$

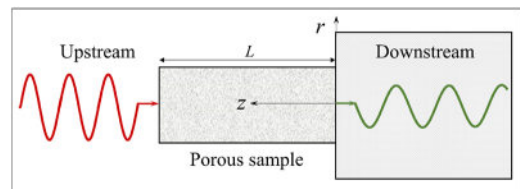


FIG. 2. Schematic of the pressure oscillation method. Upstream provides a stable oscillating pressure. After passing through a porous medium, it induces pressure oscillations in the downstream chamber.

where $\tilde{\omega} = \frac{8\bar{u}L^2}{R^2 P_0} \omega$, $\beta = \frac{P_0}{P_A}$. The downstream outlet is connected to a chamber of fixed volume, which allows boundary conditions utilizing the conservation of mass. The variation of mass inside the downstream chamber with time is equal to the fluid flow entering the downstream chamber from the porous medium, $\frac{\partial(\rho_d V_d)}{\partial t} = -\left(\bar{\rho} \bar{u}^{(0)} \cdot \bar{u}\right)\Big|_{z=0} N\pi R^2$, where ρ_d is the density of the gas in the downstream chamber and V_d is the volume of the downstream chamber. Since the density is directly proportional to pressure, substituting the averaged velocity $\bar{u}^{(0)}$ from (16), the downstream dimensionless boundary condition can be expressed as

$$\frac{\partial \bar{P}^{(0)}}{\partial \bar{t}} = \frac{N\pi R^2 L}{8V_d} \frac{8\bar{u}\bar{u}L}{R^2 P_A} \frac{\bar{P}^{(0)}}{P_0} \frac{\partial \bar{P}^{(0)}}{\partial \bar{z}} F(Kn), \quad (19)$$

where $F(Kn) = 1 + 4Kn$ is a function of the Knudsen number and $\bar{P}^{(0)}$ is the average pressure. Due to the system pressure oscillating around the equilibrium pressure P_0 , it is physically reasonable to assume that $\frac{\bar{P}^{(0)}}{P_0} \approx 1$. Combining the previous magnitude analysis $\frac{R^2 P_A}{\bar{u} L} \approx 1$, the above boundary condition Eq. (19) can be simplified to

$$\frac{\partial \bar{P}^{(0)}}{\partial \bar{t}} \Big|_{\bar{z}=0} = aF(Kn) \frac{\partial \bar{P}^{(0)}}{\partial \bar{z}} \Big|_{\bar{z}=0}, \quad (20)$$

where $a = \frac{N\pi R^2 L}{V_d}$ represents the ratio of the porous sample's pore volume to the volume of the downstream chamber. $\bar{z} = 0$ indicates the downstream outlet. In addition, the entire system is at equilibrium pressure P_0 before the start of the oscillation. Therefore, the dimensionless initial condition is

$$\bar{P}(\bar{z}, 0) = \beta. \quad (21)$$

Due to the nonlinearity of the boundary conditions at the upstream inlet, the Laplace transformation is used to solve Eqs. (17), (18), (20), and (21), and the detailed solution procedure is provided in the Appendix. After obtaining the dimensionless analytical solution, it needs to be re-scaled with some parameters to restore dimensional forms. Considering that the compressibility of the fluid is much greater than that of the porous medium skeleton, this study only considers the compressibility factor of the fluid, which is approximated by the reciprocal of the equilibrium pressure, $C_f \approx \frac{1}{P_0}$. Therefore, the storage capacity of the fluid system per unit volume of the sample can be expressed as $\beta_s = \varphi C_f = \frac{\varphi}{P_0}$. In addition, the storage capacity of the downstream chamber is represented by the ratio of the downstream chamber volume to the equilibrium pressure $\beta_d = \frac{V_d}{P_0}$. Combining these relations with Eq. (1), the analytical solution for the system of equations is obtained,

$$P(z, t) = P_0 + P_A |\alpha| \sin(\omega t + \delta + \theta) + 2P_A K \beta_s A L \sum_{n=1}^{\infty} \frac{(\beta_s L^2 \omega \cos \delta - K \psi_n^2 \sin \delta) \left[\cos(\psi_n \frac{z}{L}) - \frac{\beta_d \psi_n}{\beta_s A L} \frac{1}{F} \sin(\psi_n \frac{z}{L}) \right]}{(K^2 \psi_n^4 + \beta_s^2 L^4 \omega^2) \left[(\frac{1}{F} \beta_d \psi_n^2 - \beta_s A L) \cos \psi_n + \psi_n \sin \psi_n (\beta_s A L + \beta_d \frac{2}{F}) \right]} \psi_n^2 e^{-\frac{\kappa \psi_n^2 t}{L^2 \beta_s}}, \quad (22)$$

where $K = \frac{k}{\mu}$, ψ_n is the roots of the transient part poles, satisfying the equation $\tan \psi_n = \frac{aF}{\psi_n}$, and A is the cross-sectional area of the porous medium. $|\alpha|$ and θ are the amplitude ratio and the phase difference of pressure oscillations at position z to the upstream inlet, respectively, which are the modulus and argument of a complex number,

$$|\alpha| = \left| \frac{\kappa'(1+i) \cosh[\kappa'z(1+i)] + \frac{i\omega\beta_d}{AKF} \sinh[\kappa'z(1+i)]}{\kappa'(1+i) \cosh[\kappa'L(1+i)] + \frac{i\omega\beta_d}{AKF} \sinh[\kappa'L(1+i)]} \right|, \quad (23)$$

$$\theta = \arg \left\{ \frac{\kappa'(1+i) \cosh[\kappa'z(1+i)] + \frac{i\omega\beta_d}{AKF} \sinh[\kappa'z(1+i)]}{\kappa'(1+i) \cosh[\kappa'L(1+i)] + \frac{i\omega\beta_d}{AKF} \sinh[\kappa'L(1+i)]} \right\}, \quad (24)$$

where $\kappa' = \sqrt{\frac{\beta_s \omega}{2K}}$, and a dimensionless number is defined as $\kappa = \kappa' L$.

In Eq. (22), the first term represents the equilibrium pressure, around which the system pressure oscillates as a whole. The second term is the periodic part following the sinusoidal input from the upstream boundary. The third term is the transient part of the solution, gradually decaying with time. The analytical solution in this study is consistent with the expression derived by Fisher (1992) based on macroscopic diffusion equations. Meanwhile, the slip effect is reflected in the parameter F in the periodic part and in F and ψ_n in the transient part. This indicates that the derivation

based on the capillary model incorporating the perturbation analysis not only reproduces the analytical solution consistent with macroscopic approaches but also rationally introduces slip boundary conditions, theoretically elucidating the manifestation of the slip effect in the pressure oscillation process.

III. PERMEABILITY CALCULATION AND SLIP CORRECTION

A. Periodic solution

In experiments, by recording the amplitude ratio $|\alpha|$ and the phase difference θ between upstream and downstream, permeability k and porosity φ can be obtained using the periodic solution. When the measurement point is at the upstream inlet and downstream outlet ($z = 0$), the $|\alpha|$ and θ can be expressed as

$$|\alpha| = \left| \frac{\kappa'(1+i)}{\kappa'(1+i) \cosh[\kappa'L(1+i)] + \frac{i\omega\beta_d}{AKF} \sinh[\kappa'L(1+i)]} \right|, \quad (25)$$

$$\theta = \arg \left\{ \frac{\kappa'(1+i)}{\kappa'(1+i) \cosh[\kappa'L(1+i)] + \frac{i\omega\beta_d}{AKF} \sinh[\kappa'L(1+i)]} \right\}. \quad (26)$$

The complex number in the above equation can be represented in a complex form involving X_D and Y_D ,

$$\frac{X_D + Y_D}{X_D^2 + Y_D^2} + \frac{X_D - Y_D}{X_D^2 + Y_D^2} i, \quad (27)$$

where X_D and Y_D are the functions of two dimensionless numbers, κ and χ ,

$$X_D = \cosh(\kappa) \cos(\kappa) - \sinh(\kappa) \sin(\kappa) - \chi \cosh(\kappa) \sin(\kappa), \quad (28)$$

$$Y_D = \cosh(\kappa) \cos(\kappa) + \sinh(\kappa) \sin(\kappa) + \chi \sinh(\kappa) \cos(\kappa), \quad (29)$$

where $\chi = \frac{\omega \beta_d}{\kappa' AKF}$ and $\kappa = L \sqrt{\frac{\beta_s \omega}{2K}}$ are the dimensionless numbers. The amplitude ratio $|\alpha|$ and the phase difference θ are, respectively, the modulus and argument of the complex number in Eq. (27),

$$|\alpha| = \sqrt{\frac{2}{X_D^2 + Y_D^2}}, \quad \theta = \arctan\left(\frac{X_D - Y_D}{X_D + Y_D}\right). \quad (30)$$

Thus, by inversely solving for the two dimensionless numbers κ and χ , expressions for permeability and porosity can be obtained,

$$k = \frac{\mu L \omega \beta_d}{AF \chi \kappa}, \quad \varphi = \frac{2\kappa V_d}{AFL \chi}. \quad (31)$$

So far, after the amplitude ratio $|\alpha|$ and the phase difference θ are obtained in the experiment, by inversely solving the system of

Eq. (30) and the system of Eqs. (28) and (29), dimensionless numbers κ and χ can be determined. Subsequently, permeability and porosity can be further calculated using Eq. (31).

By varying the parameter F , the slip correction method in the periodic solution for calculating permeability can be analyzed. In Eq. (31), considering F as a function of the Kn number, the intrinsic permeability k_{int} is calculated. If $F = 1$ ($Kn = 0$), the apparent permeability can be expressed as $k_{app} = \frac{\mu L \omega \beta_d}{A \chi \kappa}$. By comparing the expressions for apparent permeability and intrinsic permeability, it can be deduced that $k_{app} = k_{int}(1 + 4Kn)$. Combining the definition of Knudsen number, $Kn = \frac{\lambda}{R}$, where the mean free path λ is inversely proportional to the average pressure, the relationship is equivalent to the Klinkenberg formula $k_{app} = k_{int}\left(1 + \frac{b}{p}\right)$. This indicates that the periodic solution in the pressure oscillation method is theoretically a pseudo-steady-state form, and the Klinkenberg formula can be directly used to correct the slip effect on permeability.

B. Transient solution

According to the analytical solution (22) derived above, the downstream pressure in the pressure oscillation method exhibits both periodic and transient parts. However, previous studies have been limited to considering only the periodic term. In this study, a reasonable method of using the transient term based on the periodicity of the pressure oscillation method is proposed. The transient term is essentially a summation series of exponential functions about time, decaying as time progresses. Since the detected periodic term of the downstream chamber remains consistent across different cycles, taking the difference between two cycles allows only the transient term to be retained,

$$\Delta_T P(0, t) = P(0, t) - P(0, t + T) = 2P_A K \beta_s AL \sum_{n=1}^{\infty} \frac{(\beta_s L^2 \omega \cos \delta - K \psi_n^2 \sin \delta) \psi_n^2 \left(1 - e^{-\frac{K \psi_n^2 T}{L^2 \beta_s}}\right) e^{-\frac{K \psi_n^2 t}{L^2 \beta_s}}}{(K^2 \psi_n^4 + \beta_s^2 L^4 \omega^2) \left[\left(\frac{1}{F} \beta_d \psi_n^2 - \beta_s AL\right) \cos \psi_n + \psi_n \sin \psi_n (\beta_s AL + \beta_d \frac{2}{F})\right]}. \quad (32)$$

Since the roots ψ_n for $n > 1$ are significantly smaller than the first term ψ_1 for $n = 1$, the summation series can be approximated by considering only the first term. Thus, the periodic pressure difference can be expressed as

$$\Delta_T P(0, t) = \frac{2P_A K \beta_s AL (\beta_s L^2 \omega \cos \delta - K \psi_1^2 \sin \delta) \psi_1^2 \left(1 - e^{-\frac{K \psi_1^2 T}{L^2 \beta_s}}\right) e^{-\frac{K \psi_1^2 t}{L^2 \beta_s}}}{(K^2 \psi_1^4 + \beta_s^2 L^4 \omega^2) \left[\left(\frac{1}{F} \beta_d \psi_1^2 - \beta_s AL\right) \cos \psi_1 + \psi_1 \sin \psi_1 (\beta_s AL + \beta_d \frac{2}{F})\right]}. \quad (33)$$

The above periodic pressure difference is solely an exponential function of time and taking the logarithm of it can be expressed as a linear function of time,

$$\ln \Delta_T P(0, t) = \ln M + Nt, \quad (34)$$

where

$$M = \frac{2P_A K \beta_s AL^3 \omega \psi_1^2 \left(1 - e^{-\frac{K \psi_1^2 T}{L^2 \beta_s}}\right)}{(K^2 \psi_1^4 + \beta_s^2 L^4 \omega^2) \left[\left(\frac{1}{F} \beta_d \psi_1^2 - \beta_s AL\right) \cos \psi_1 + \psi_1 \sin \psi_1 (\beta_s AL + \beta_d \frac{2}{F})\right]}, \quad (35)$$

$$N = -\frac{K \psi_1^2}{L^2 \beta_s}. \quad (36)$$

The N is the slope obtained by fitting the logarithmic periodic pressure difference from experimental data. Inverting the expression of

N and substituting the definitions of K and β_s , the following formula for permeability can be obtained:

$$k = -\frac{N\mu L^2 \varphi}{\psi_1^2 P_0}. \quad (37)$$

Based on the above data processing procedure, a method for using transient solutions in pressure oscillation experiments is established. Generally, the periodic term used by previous researchers requires pressure data after the transient term has decayed away to calculate the amplitude ratio and phase difference. The transient method requires pressure data where the transient term is present, and the pressure difference over the first two periods is optimal. This compensates for the neglect of the initial period and may offer a quicker measurement under suitable conditions. Unfortunately, this method also retains the disadvantages of the transient method, similar to the pulse decay method, which is sensitive to the effects of external fluctuations and parameter changes.

Similar to the periodic solution, the transient solution takes into account the influence of the slip effect. The parameter F associated with the slip effect appears in the equation for solving the parameter ψ_1 , $\tan \psi_1 = \frac{aF}{\psi_1}$. The permeability k in Eq. (37) should be the intrinsic permeability. If $F = 1$, neglecting the slip effect, then determining ψ_1' involves solving $\tan \psi_1' = \frac{a}{\psi_1}$, and the calculated permeability is referred to as the apparent permeability,

$$k' = -\frac{N\mu L^2 \varphi}{\psi_1'^2 P_0}. \quad (38)$$

By comparing (37) with (38), the relationship between the apparent permeability and the intrinsic permeability for the transient solution can be expressed as

$$\frac{k'}{k} = \frac{\psi_1^2}{\psi_1'^2}. \quad (39)$$

If consistency with the Klinkenberg correction relationship is desired, the condition $\frac{\psi_1^2}{\psi_1'^2} = F$ needs to be satisfied. Combining the equation for ψ_1 , an equivalent form of the assumed condition can be obtained, $1 - F \frac{(\tan \psi_1')^2}{(\tan \psi_1)^2} = 0$. Therefore, this study defines a criterion as

$$\Gamma = 1 - F \frac{(\tan \psi_1')^2}{(\tan \psi_1)^2}. \quad (40)$$

The closer this criterion is to 0, the higher the approximate validity of the assumption and the more accurate the intrinsic permeability obtained using the Klinkenberg correction. The relationship $\Gamma \sim (a, Kn)$ between the criterion Γ and the volume ratio a and the Knudsen number Kn can be obtained through numerical solving of the equations for parameters ψ_1 and ψ_1' is shown in Fig. 3. The smaller the Knudsen number, the less impact on the criterion. If the maximum Kn considered is 1, then when $a < 0.01$, the criterion Γ is less than 0.014. For slip flow, which typically considers a maximum Kn of 0.1, corresponding to a criterion less than 0.013, $a < 0.1$ is sufficient. Therefore, the selection of the value for a should be based on a comprehensive consideration of the acceptable level of

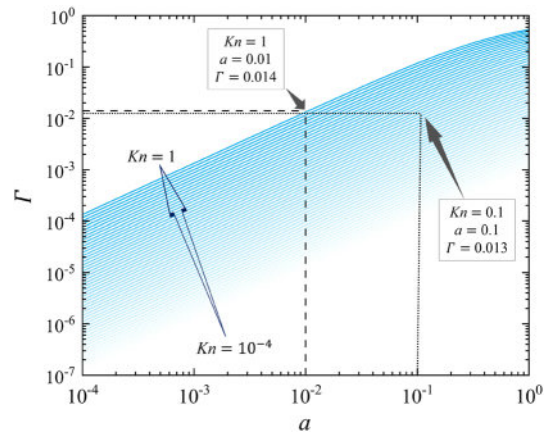


FIG. 3. Variation of the criterion Γ with the volume ratio a and Knudsen number Kn . The highlighted points emphasize that when $a < 0.01$, the criterion $\Gamma < 0.014$, with the Knudsen number up to 1. When $a < 0.1$, the criterion $\Gamma < 0.013$, with the Knudsen number up to 0.1.

error and the magnitude of slip effects. If a more stringent criterion is required, a smaller a would be needed to fulfill the requirement, ensuring a more accurate use of the Klinkenberg correction relationship.

IV. EXPERIMENTAL VALIDATION

To validate the explanation of the slip effect in the periodic solution and the proposed transient solution method above, a permeability measurement platform is established as shown in Fig. 4. The platform is capable of implementing three measurement methods: the steady-state method, pulse decay method, and pressure oscillation method. The porous sample is made of polymer material and put into a metal nut, and the whole nut is put into a sealed chamber. Details of the sample and experimental setup parameters are provided in Table I. The porosity in the table is determined through the mercury intrusion method, which provides input parameters for the pulse decay method.

A. Comparison of different methods

The measurement on sample 1 is conducted using the pressure oscillation method, with the equilibrium pressure set at 2×10^5 Pa, and the upstream and downstream pressure results are shown in Fig. 5(a). Due to the damping effect of the porous sample, there is a noticeable decay in amplitude and phase shift between the upstream and downstream pressure. The downstream pressure between the first two periods exhibits amplitude decay, as illustrated in the magnified plot in Fig. 5(b). Subsequently, experiments are conducted with seven different equilibrium pressures, and the resulting downstream pressure curves are presented in Fig. 5(c). The amplitude ratios and phase differences are determined by the Fast Fourier Transform (FFT) and the apparent permeability k_{app} is calculated based on Eq. (31). Combining the reciprocal of the pore equilibrium pressure and applying the Klinkenberg correction yields the intrinsic permeability k_{int} , as shown in Fig. 5(d). The fitting coefficient

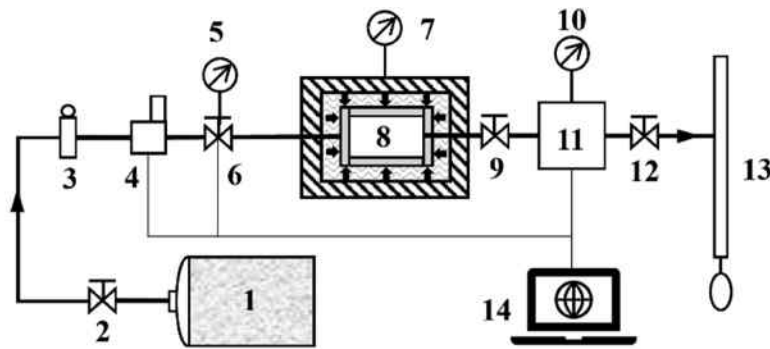


FIG. 4. Schematic diagram of the permeability measurement platform.

- | | | |
|----------------------------|-------------------------------|---------------------------|
| 1. Compressor | 6. Upstream valve | 11. Downstream chamber |
| 2. intake shut-off valve | 7. Confining pressure gauge | 12. Outlet shut-off valve |
| 3. Pressure regulator | 8. Porous sample holder | 13. Soap film flowmeter |
| 4. Oscillation generator | 9. Downstream valve | 14. Data collection |
| 5. Upstream pressure gauge | 10. Downstream pressure gauge | |

TABLE I. Parameters of the sample and the experiment setup.

Sample		Experimental setup	
Material	Polymer	Upstream volume (m ³)	1.4988 × 10 ⁻⁶
Test gas	Air	Initial period (min)	30
Sample length (m)	6.50 × 10 ⁻³	Upstream amplitude (Pa)	40 000
Sample cross section radius (m)	1.10 × 10 ⁻³	Acquisition interval (s)	0.5
Sample 1 porosity (%)	0.131	Initial phase	0

$R^2 = 0.9998$, indicating a high level of fit linearity, thus enhancing the credibility of the results.

Using the transient solution, permeability can also be calculated on the same set of experimental data. Following Eq. (34), the logarithm of the difference between the first two periods of the downstream pressure exhibits a linear relationship over time, as depicted in Fig. 6(a). The increased dispersion in the later data within a single period indicates that, after the exponential term in the analytical solution decays with time, the random error in periodic pressure difference will increase. This also suggests that under extremely short-period conditions, the transient solution may be unusable due to significant errors. After fitting the logarithmic periodic pressure difference and obtaining the slope, the apparent permeability k_{app} can be inversely calculated using Eq. (38). The Klinkenberg-corrected results of the transient solution are presented in Fig. 6(b), where the intercept represents the intrinsic permeability of the transient solution.

Comparing the intrinsic permeability obtained from the periodic solution and the transient solution, the relative error is only 0.24%, indicating a high level of agreement between the two methods and validating the effectiveness of the transient solution proposed in this study. Furthermore, the comparison of the apparent permeability obtained under the same pore pressure using the two methods is shown in Fig. 7. The results from both solutions generally cluster around a line with a slope of 1, but the apparent permeability from the periodic solution is slightly larger than that

from the transient solution. The reason for this phenomenon lies in the fact that the decay of the transient term can only approach zero infinitely. The data used for calculating the periodic solution may include slight transient terms, causing the amplitude ratio obtained from FFT calculations to be larger, thus resulting in a larger permeability. However, this does not significantly affect the calculation of the intrinsic permeability. Therefore, the periodic solution is theoretically affected by the incompletely decaying transient solution, reflecting the slight theoretical advantage of the transient solution, although this effect may be negligible in experiments. In addition, since the pressure difference over two cycles can be calculated from any point, the proposed transient solution avoids instantaneous fluctuations when the valve opens.

To further validate the accuracy of the pressure oscillation method, this study made additional improvements to the experimental setup and conducted low-pressure pulse decay experiments. The experiment employed an upstream constant pressure scheme, as illustrated in Fig. 8(a). Tests are conducted under the same pulse pressure at nine different constant upstream pressures. The permeability calculations referenced the formulas provided by Metwally and Sondergeld (2011). Applying the Klinkenberg correction to the apparent permeability is illustrated in Fig. 8(b). Comparing the experimental results of the pulse decay method and the pressure oscillation method, as shown in Table II, the relative error of the two methods is within 4%.

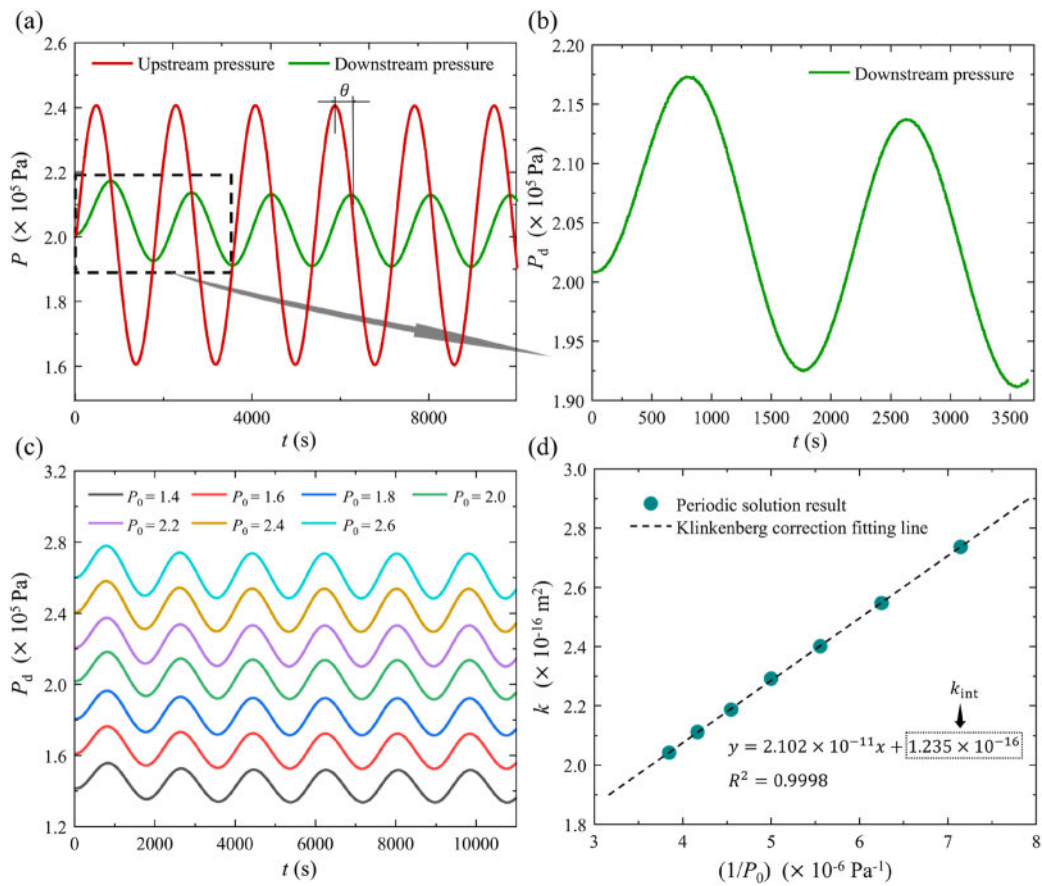


FIG. 5. Experimental results of the pressure oscillation method. (a) Upstream and downstream pressure curves with an equilibrium pressure of 2×10^5 Pa. (b) Enlarged image of downstream pressure curves for the first two periods. (c) Downstream pressure curves at seven different equilibrium pressures. (d) Klinkenberg-corrected results of the periodic solution with the equation representing a linear fit result, where the intercept is the intrinsic permeability.

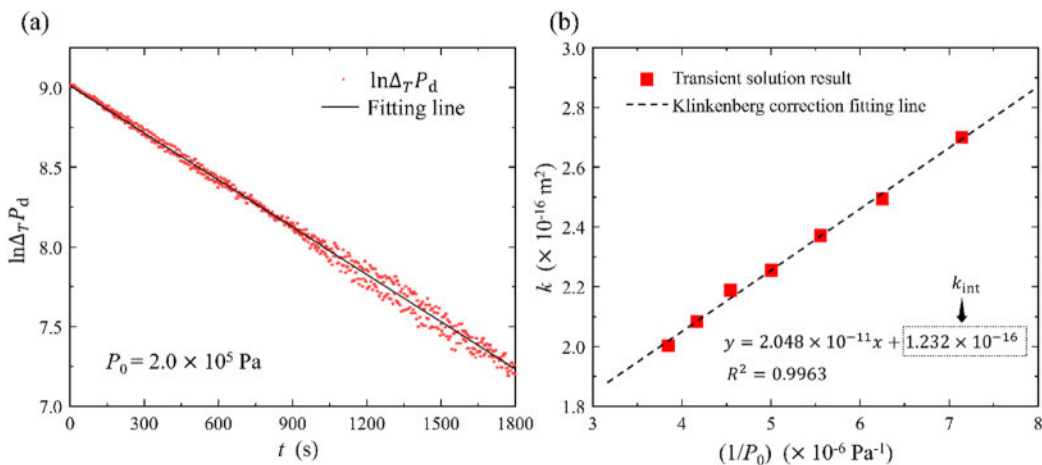


FIG. 6. Processing results of the transient solution in the pressure oscillation method. (a) Linear variation of logarithmic periodic pressure difference over time. (b) Klinkenberg-corrected results of the transient solution, with the equation representing a linear fit result, where the intercept is the intrinsic permeability.

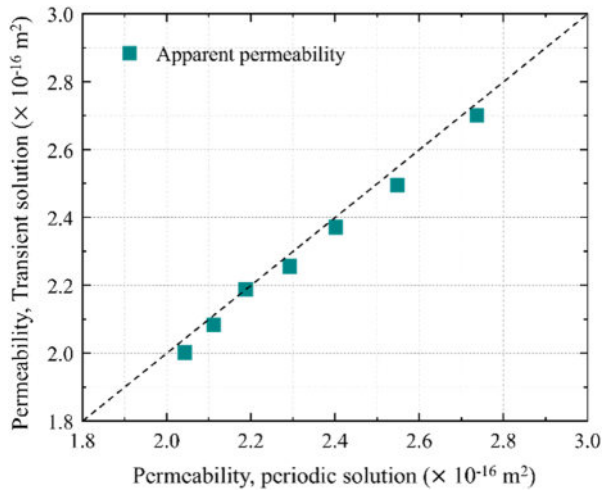


FIG. 7. Comparison of apparent permeability results between the periodic solution and the transient solution.

B. Measurement duration

The measurement duration for the pressure oscillation method depends on the chosen length of the period. For the periodic solution, one period after eliminating the transient term is sufficient to obtain the amplitude ratio and the phase difference theoretically. In this study, a higher level of precision is achieved by considering two periods after removing the first two, so the duration can be considered as four periods. The transient solution typically involves the first two periods, so its duration can be considered as the time required for two periods.

This study employed measurements with varying period duration at a consistent equilibrium pressure of 2×10^5 Pa. Sample 1 is measured using 13 different periods ranging from a minimum

TABLE II. Comparison of results from three methods.

Method		Intrinsic permeability ($\times 10^{-16} \text{ m}^2$)	Relative error
Pressure oscillation method	Pulse decay	1.281	...
	Periodic solution	1.235	3.59%
	Transient solution	1.232	3.83%

of 1 min to a maximum of 45 min, and the amplitude ratio and the phase difference are calculated as illustrated in Fig. 9(a). The amplitude ratio increases with increasing period, attributed to the longer reaction time in the downstream chamber, resulting in higher amplitudes. Concurrently, the phase difference decreases with increasing period, with a conversion applied for negative phase difference. Permeability values are calculated for both the periodic solution and the transient solution using data corresponding to different periods, and the results are presented in Fig. 9(b). The permeability from the periodic solution stabilizes around an average of $2.263 \times 10^{-16} \text{ m}^2$, and its corresponding minimum period of 1 min remains plausible. The amplitude ratio at the minimum period is merely 0.01, reaching the minimum resolution of the sampling instrument. Therefore, the minimum usable period for the periodic solution depends on the sampling resolution's ability to detect the amplitude ratio accurately. The results of the transient solution fluctuate slightly but are overall within 10% of the deviation from the mean error. However, the transient terms are minimal at shorter periods, causing negative values in the periodic pressure difference due to random error, which prevents the calculation of permeability. The permeability measured for sample 1 under a 5-min period condition has exhibited a significant deviation, and under conditions less than 5 min, fitting calculations

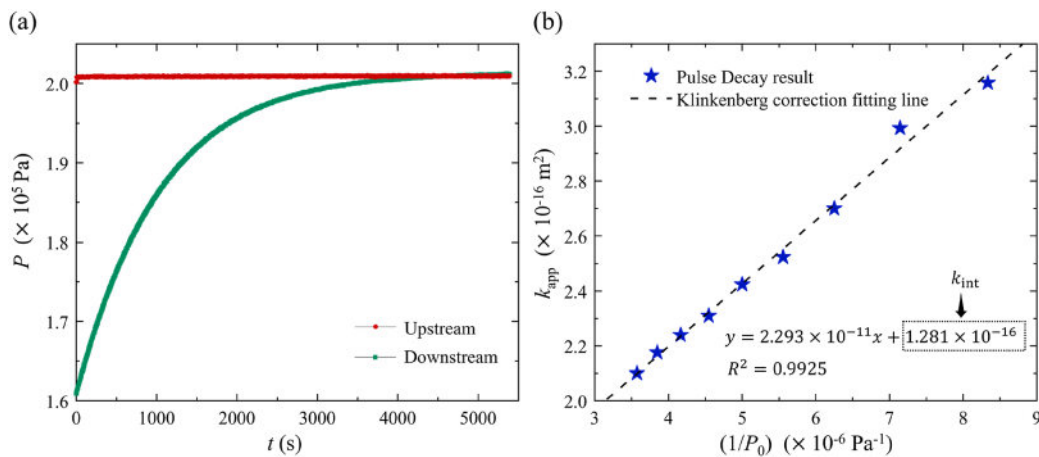


FIG. 8. Results of pulse decay experiment. (a) Upstream and downstream pressure curves. (b) Klinkenberg-corrected results of the pulse decay method, with the equation representing a linear fit result, where the intercept is the intrinsic permeability.

TABLE III. Comparison of the measurement duration for different methods.

Method	Sample 1 (10^{-16} m^2)	Sample 2 (10^{-18} m^2)
Conventional pulse decay	At least 40 min	88 h
Periodic solution	4 min	24 h
Transient solution	20 min	...

are no longer feasible. Hence, the minimum usable period for the transient solution is contingent upon the ability to accurately detect the decay of transient terms. The measurement duration in the conventional pulse decay method is determined by achieving equilibrium pressure.

To further compare the measurement duration, measurements are conducted on sample 2 with lower permeability, and results for both samples are summarized in Table III. A comparison reveals that the measurement duration for periodic solution in the pressure oscillation method is significantly shorter than that in the pulse decay method, with an approximately tenfold increase in measurement speed for sample 1. The measurement speed for the transient solution has increased by approximately two times. In sample 2 with lower permeability, the measurement speed has increased by at least threefold. Due to the placement of the measurement apparatus indoors, it is not possible to ensure a completely constant temperature. For ultra-low permeability samples, the longer measurement duration amplifies the impact of temperature instability, leading to significant errors in the pulse decay method. In addition, the transient solution of the pressure oscillation method is rendered unusable due to the influence of temperature fluctuations. This observation highlights the low sensitivity of the periodic solution to random errors, indicating its strong robustness.

C. Parameter regulation

The challenge in the pressure oscillation method lies in selecting appropriate parameters to obtain a detectable amplitude ratio

and phase difference. The factors influencing the amplitude ratio and the phase difference mainly include sample parameters [permeability (k) and porosity (ϕ)] and experimental setup parameters [period (T) and downstream chamber volume (V_d)], corresponding to the frequency (ω) and downstream volume ratio (a) used in the calculation process. By inversely solving Eqs. (28)–(30), the impact of different parameters on the detection results can be analyzed.

An analysis of the effects of changes in permeability and porosity is conducted. Based on the experimental results of sample 1 above, the 30-min period is selected, varying the porosity from 0.01 to 0.6 and the permeability from 10^{-18} m^2 to 10^{-12} m^2 . The resulting changes in amplitude ratio and phase difference are shown in Fig. 10. The results show that the sensitivity of the amplitude ratio and the phase difference to porosity is extremely low, and the variation is less than 0.5% due to a wide range of porosity changes. In other words, the minimal errors in the amplitude ratio and the phase difference during measurement will be magnified in the error of porosity. This is the fundamental reason for the inaccuracy of porosity measurements and also explains the experimental results reported by Hasanov *et al.* (2017), in which storage capacity measurements were extremely inaccurate. Permeability significantly influences amplitude ratio and phase difference, exhibiting a clear trend. Therefore, when considering parameter regulation, the influence of porosity can be neglected, and only permeability is considered.

In the calculation process of the periodic solution, two dimensionless numbers, χ and κ , ultimately transform the amplitude ratio and phase difference into permeability and porosity. The variation of the three main parameters—period, downstream volume, and permeability—can be transformed into the variation of two dimensionless numbers. The period is taken from 60 to 108 000 s (1 min to 30 h), downstream volume ranges from 10^{-16} to 10^4 m^3 , and permeability ranges from 10^{-21} to 10^{-12} m^2 (1 nD to 1D). The contour of the amplitude ratio with the two dimensionless numbers is displayed in Fig. 11. Depending on the accuracy of the experimental equipment, a usable amplitude ratio can be selected in the range of, for example, 0.01 to 0.99 in Fig. 11. Based on the estimated

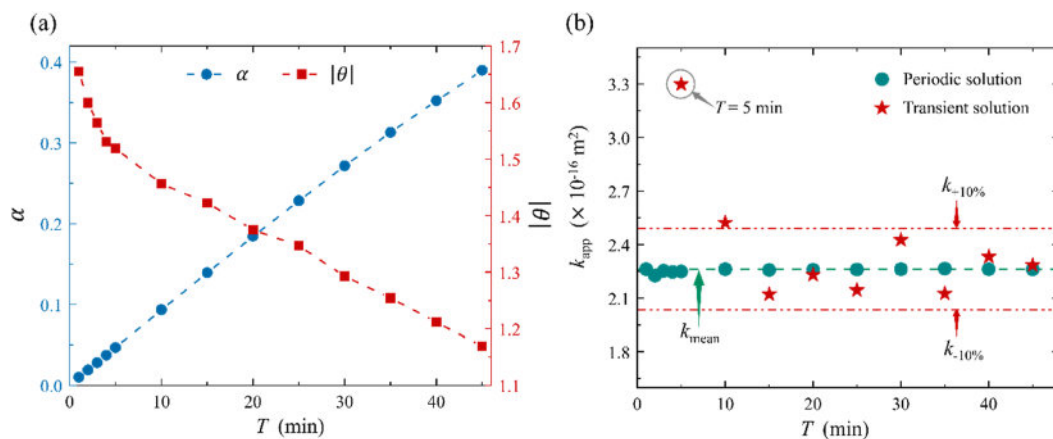


FIG. 9. Experimental results for sample 1 at the same equilibrium pressure with different periods: (a) Amplitude ratio and phase difference and (b) permeability from the periodic and the transient solution. The permeability measured for sample 1 under a 5-min period condition has exhibited a significant deviation.

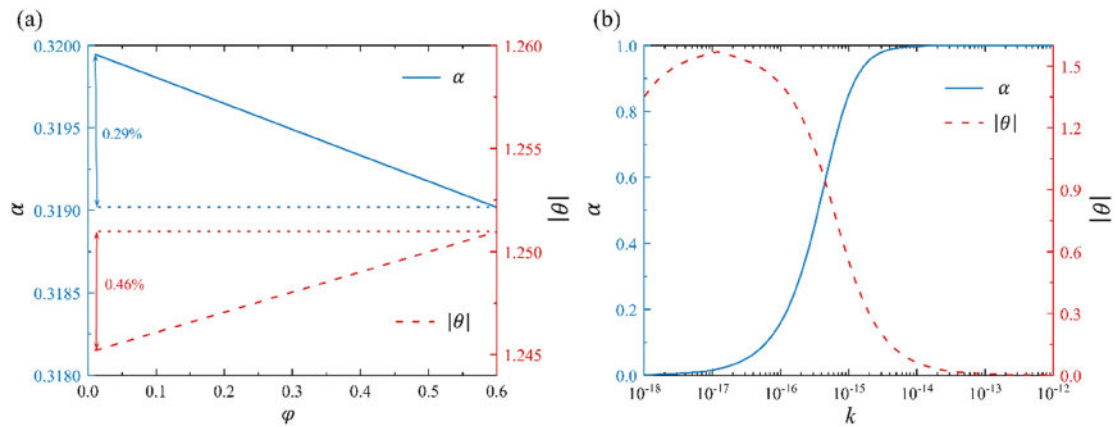


FIG. 10. Variation curves of amplitude ratio and phase difference with (a) permeability and (b) porosity. The percentage in panel (a) represents the maximum change in amplitude ratio and phase difference caused by a change in porosity from 0.01 to 0.6.

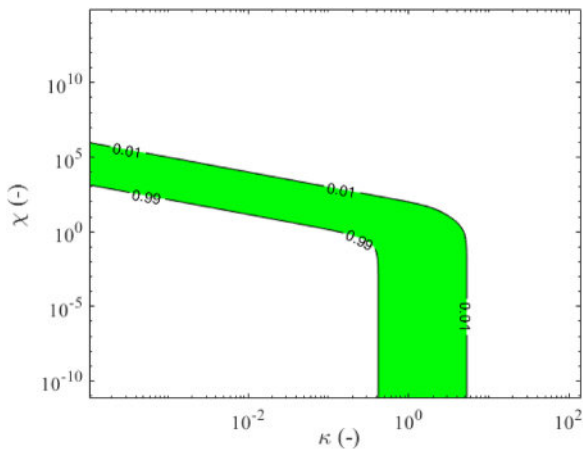


FIG. 11. Contour of amplitude ratio with two dimensionless numbers.

magnitude of permeability, appropriate measurement periods and downstream volumes can be chosen. A reasonable amplitude ratio can be obtained by ensuring that the values of the two dimensionless numbers are within the corresponding ranges.

Finally, a sensitivity analysis of the input parameters for the periodic solution is necessary for the evaluation of this method (Jannot *et al.*, 2008; Jannot *et al.*, 2007). The inversion process for the periodic solution entails the transformation from measured quantities ($|\alpha|$ and θ) to dimensionless numbers (κ and χ), and the input parameter influences exist only in the inversion process from dimensionless numbers to permeability (k) and porosity (φ) as depicted in Eq. (31). The parameters involved here include sample parameters (diameter D and length L), experimental setup parameters (equilibrium pressure P_0 and angular velocity ω), and downstream chamber volume V_d . One advantage of the pressure oscillation method is extremely low sensitivity to fluctuations in environmental or internal parameters since it considers the relative values of amplitude

and phase generated by the upstream and downstream over multiple cycles. Hence, errors arising from fluctuations in equilibrium pressure and angular frequency can be neglected. In Eq. (31), the sample length L and downstream chamber volume V_d are directly proportional to permeability, and the percentage deviation can be directly related to permeability. Smaller samples are more difficult to process, leading to increased length errors, typically controlled within 3%. Smaller downstream chamber volumes result in higher percentage errors but should be kept within 5%. The errors arising from the ratio of the two to permeability are within 5%. The square of the sample diameter is inversely proportional to permeability, with sensitivity higher than that of length. A 5% deviation of diameter will result in approximately a 10% permeability error. Therefore, attention should be paid to the processing precision of porous sample size and measurement accuracy during the usage of this method.

V. CONCLUSIONS

This study presents the theoretical foundation with the Klinkenberg correction for the pressure oscillation method based on the capillary model. The periodic solution in the pressure oscillation method conforms to the slip correction form of the steady-state method and can directly employ the Klinkenberg correction. A method for utilizing the transient solution in pressure oscillation experiments is proposed, confirming its applicability with limitations when utilizing the Klinkenberg correction. The introduction of this method achieves a unified approach for both quasi-steady-state and unsteady-state methods in the pressure oscillation technique. The experimental validation has affirmed the consistency between transient and periodic solutions.

In contrast to the pulse decay method, the pressure oscillation technique exhibits advantages in terms of measurement duration. Under conditions of higher permeability, a tenfold increase in measurement speed can be attained, while under lower permeability conditions, there is a minimum threefold improvement. Through the inverse solution process for permeability calculation, this study analyzed the main factors influencing measurements in the pressure

oscillation method. The reason for the inaccuracy of porosity measurement is that porosity is extremely sensitive to the amplitude ratio and the phase difference, and the measurement error is magnified several times. The contour of the amplitude ratio response based on the dimensionless number is established to provide a reference for the selection of experimental parameters for engineering practice.

ACKNOWLEDGMENTS

This work was financially supported by the NSF grant of China (Grant Nos. U1837602 and 12272207) and the Tsinghua University Initiative Scientific Research Program.

AUTHOR DECLARATIONS

Conflict of Interest

The authors have no conflicts to disclose.

Author Contributions

Mingbao Zhang: Investigation (equal); Validation (equal); Writing – original draft (equal). **Zhiguo Tian:** Investigation (equal); Software (equal); Writing – review & editing (equal). **Moran Wang:** Conceptualization (equal); Supervision (equal); Writing – review & editing (equal).

DATA AVAILABILITY

The data that support the findings of this study are available from the corresponding author upon reasonable request.

APPENDIX: ANALYTICAL SOLUTION DERIVATION USING LAPLACE TRANSFORM

First, perform the Laplace transform on the equations and boundary conditions. The transformed time variable is denoted as σ , yielding

$$\frac{\partial^2 \bar{P}}{\partial \bar{z}^2} - q^2 \bar{P} + \beta = 0, \quad \bar{P}|_{\bar{z}=1} = \frac{\bar{\omega} \cos(\delta) + \sigma \sin(\delta)}{\sigma^2 + \bar{\omega}^2} + \frac{\beta}{\sigma}, \quad (A1)$$

$$\left. \frac{d\bar{P}}{d\bar{z}} \right|_{\bar{z}=0} - \frac{\sigma}{aF} \bar{P}|_{\bar{z}=0} + \frac{1}{aF} = 0,$$

where $q = \sqrt{\sigma}$, and the parameters with an overline represent the Laplace-transformed quantities. The general solution of Eq. (A1) is

$$\bar{P}(\bar{z}, \sigma) = C_1 e^{-q\bar{z}} + C_2 e^{q\bar{z}} + \frac{\beta}{q^2}. \quad (A2)$$

Substituting the boundary conditions yields

$$\bar{P}(\bar{z}, \sigma) = \frac{\bar{\omega} \cos(\delta) + \sigma \sin(\delta)}{\sigma^2 + \bar{\omega}^2} \frac{q \cosh(q\bar{z}) + \lambda \sigma \sinh(q\bar{z})}{q \cosh(q) + \lambda \sigma \sinh(q)} + \frac{\beta}{q^2}, \quad (A3)$$

where $\lambda = \frac{1}{bF}$. Subsequently, proceed with the inverse Laplace transform using the following general inversion formula:

$$\tilde{P}(\bar{z}, t) = \frac{1}{2\pi i} \int_{c-i\infty}^{c+i\infty} \bar{P}(\bar{z}, \sigma) e^{\sigma t} d\sigma. \quad (A4)$$

Substituting Eq. (A3) yields

$$\tilde{P}(\bar{z}, t) = \frac{1}{2\pi i} \int_{c-i\infty}^{c+i\infty} \frac{\bar{\omega} \cos(\delta) + \sigma \sin(\delta)}{\sigma^2 + \bar{\omega}^2} \frac{q \cosh(q\bar{z}) + \lambda \sigma \sinh(q\bar{z})}{q \cosh(q) + \lambda \sigma \sinh(q)} d\sigma + \beta, \quad (A5)$$

where c is a real positive constant, which is chosen to be large enough so that the singularities of the above equation are all to the left of the line $(c - i\infty, c + i\infty)$. The two poles of the product function are $\sigma_{1,2} = \pm i\bar{\omega}$, and the remaining poles σ_n are on the negative real axis. The integration path is a large semicircle of radius R surrounded by $x = c$. Then use the residue theorem,

$$\tilde{P}(\bar{z}, t) = \sum_{n=1}^{\infty} \text{Res}(\sigma_n) + \beta, \quad (A6)$$

where $\text{Res}(\sigma_n)$ is the residue calculated at the pole. The pole at $\sigma_{1,2} = \pm i\bar{\omega}$ represents the periodic components in the solution, while the pole at σ_n is a negative real number indicating the transient part of the solution decreasing with time.

Further calculating σ_n , let $q \cosh(q) + \lambda \sigma \sinh(q) = 0$, and this equation is satisfied only when q is an imaginary number. Let $q = i\psi$, where ψ is a real number. Combining the previously defined $q = \sqrt{\sigma}$ yields $\sigma_n = (i\psi)^2 = -\psi_n^2$. Substituting q and σ back into the original equation and combining the formulas $\sinh(x) = -i\sin(x)$, $\cosh(x) = \cos(ix)$, ψ_n are the root of the following expression:

$$\tan(\psi) = \frac{1}{\lambda\psi} = \frac{bF}{\psi}. \quad (A7)$$

Since the integrand can be expressed as a fraction, the residue of the transient term can be represented as

$$\text{Res}(\sigma_n) = \frac{\bar{\omega} \cos(\delta) + \sigma \sin(\delta)}{\sigma^2 + \bar{\omega}^2} \frac{q \cosh(q\bar{z}) + \lambda \sigma \sinh(q\bar{z})}{\frac{d}{d\sigma} [q \cosh(q) + \lambda \sigma \sinh(q)]} e^{\sigma t}. \quad (A8)$$

Upon substitution of the expressions for σ and λ , combined with the application of formula $(\sinh(x))' = \cosh(x)$, $(\cosh(x))' = \sinh(x)$ and subsequent simplification, the following expression is derived:

$$\text{Res}(\sigma_n) = 2\psi_n^2 \frac{\bar{\omega} \cos(\delta) - \psi_n^2 \sin(\delta)}{\psi_n^4 + \bar{\omega}^2} \frac{[\cos(\psi_n \bar{z}) - \psi_n \lambda \sin(\psi_n \bar{z})] e^{-\psi_n^2 t}}{(\lambda \psi_n^2 - 1) \cos(\psi_n) + \psi_n \sin(\psi_n) (1 + 2\lambda)}. \quad (A9)$$

Therefore, the transient part of the solution is

$$\tilde{P}_{tra} = 2 \sum_{n=1}^{\infty} \frac{(\tilde{\omega} \cos(\delta) - \psi_n^2 \sin(\delta)) [\cos(\psi_n \tilde{z}) - \psi_n \lambda \sin(\psi_n \tilde{z})]}{(\psi_n^4 + \tilde{\omega}^2) [(\lambda \psi_n^2 - 1) \cos(\psi_n) + \psi_n \sin(\psi_n) (1 + 2\lambda)]} \psi_n^2 e^{-\psi_n^2 t} \quad (A10)$$

The residue corresponding to the periodic component of $\sigma_{1,2} = \pm i\tilde{\omega}$ can be expressed as

$$\text{Res}(\sigma_n) = \frac{\tilde{\omega} \cos(\delta) + \sigma \sin(\delta)}{\frac{d}{d\sigma}(\sigma^2 + \tilde{\omega}^2)} \frac{q \cosh(q\tilde{z}) + \lambda \sigma \sinh(q\tilde{z})}{[q \cosh(q) + \lambda \sigma \sinh(q)]} e^{\sigma t} \quad (A11)$$

Since σ_1 and σ_2 are the conjugate complex numbers to each other, the solution of the periodic part can be expressed as

$$\begin{aligned} \tilde{P}_{per} &= \alpha_0(\sigma_1) \cdot \alpha(\sigma_1) + \alpha_0(\sigma_2) \cdot \alpha(\sigma_2) \\ &= \frac{1}{2i} (\alpha' \cdot \alpha(\sigma_1) - \overline{\alpha'} \cdot \alpha(\sigma_2)), \end{aligned} \quad (A12)$$

where α' and $\overline{\alpha'}$ are the conjugate complex numbers to each other, and

$$\alpha_0(\sigma_1) = \frac{\tilde{\omega} \cos(\delta) + i\tilde{\omega} \sin(\delta)}{2i\tilde{\omega}} e^{i\tilde{\omega} t} = \frac{\alpha'}{2i}, \quad (A13)$$

$$\alpha_0(\sigma_2) = \frac{\tilde{\omega} \cos(\delta) - i\tilde{\omega} \sin(\delta)}{-2i\tilde{\omega}} e^{-i\tilde{\omega} t} = \frac{\overline{\alpha'}}{-2i}, \quad (A14)$$

$$\alpha(\sigma) = \frac{q \cosh(q\tilde{z}) + \lambda \sigma \sinh(q\tilde{z})}{q \cosh(q) + \lambda \sigma \sinh(q)}. \quad (A15)$$

Equation (A12) can be reduced to taking the imaginary part of the complex number,

$$\tilde{P}_{per} = \text{Im}(\alpha' \cdot \alpha(\sigma_1)) = \text{Im}(|\alpha| e^{i(\omega t + \delta + \arg(\alpha))}) = |\alpha| \sin(\tilde{\omega} t + \delta + \theta). \quad (A16)$$

Substituting $q_1 = \sqrt{i\tilde{\omega}} = \kappa(1 + i)$ yields specific expressions for $|\alpha|$ and θ ,

$$|\alpha| = \left| \frac{\kappa(1 + i) \cosh(\kappa\tilde{z}(1 + i)) + \lambda i\tilde{\omega} \sinh(\kappa\tilde{z}(1 + i))}{\kappa(1 + i) \cosh(\kappa(1 + i)) + \lambda i\tilde{\omega} \sinh(\kappa(1 + i))} \right|, \quad (A17)$$

$$\theta = \arg \left\{ \frac{\kappa(1 + i) \cosh(\kappa\tilde{z}(1 + i)) + \lambda i\tilde{\omega} \sinh(\kappa\tilde{z}(1 + i))}{\kappa(1 + i) \cosh(\kappa(1 + i)) + \lambda i\tilde{\omega} \sinh(\kappa(1 + i))} \right\}. \quad (A18)$$

The total solution is

$$\tilde{P} = \tilde{P}_{tra} + \tilde{P}_{per} + \beta = \beta + |\alpha| \sin(\tilde{\omega} t + \delta + \theta) + 2 \sum_{n=1}^{\infty} \frac{(\tilde{\omega} \cos(\delta) - \psi_n^2 \sin(\delta)) [\cos(\psi_n \tilde{z}) - \psi_n \lambda \sin(\psi_n \tilde{z})]}{(\psi_n^4 + \tilde{\omega}^2) [(\lambda \psi_n^2 - 1) \cos(\psi_n) + \psi_n \sin(\psi_n) (1 + 2\lambda)]} \psi_n^2 e^{-\psi_n^2 t}. \quad (A19)$$

Substituting the dimensions of each parameter into Eq. (A19) leads to the derivation of Eq. (22) as presented in this paper.

REFERENCES

- Abe, J., Kawasaki, T., and Harjo, S., "Development of triaxial compressive apparatus for neutron experiments with rocks," *Rev. Sci. Instrum.* **93**, 025103 (2022).
- An, C., Killough, J., and Xia, X., "Investigating the effects of stress creep and effective stress coefficient on stress-dependent permeability measurements of shale rock," *J. Pet. Sci. Eng.* **198**, 108155 (2021).
- Assady, A., Jabbari, H., Ellafi, A. M., and Goudarzi, B., "On the characterization of bakken formation: Oscillating-pulse, pulse-decay permeability measurement and geomechanics," in 53rd U.S. Rock Mechanics/Geomechanics Symposium, 2019.
- Beloborodov, R., Pervukhina, M., and Lebedev, M., "Compaction trends of full stiffness tensor and fluid permeability in artificial shales," *Geophys. J. Int.* **212**, 1687–1693 (2018).
- Bernabé, Y., Mok, U., and Evans, B., "A note on the oscillating flow method for measuring rock permeability," *Int. J. Rock Mech. Min. Sci.* **43**, 311–316 (2006).
- Boulin, P. F., Bretonnier, P., Gland, N., and Lombard, J. M., "Contribution of the steady state method to water permeability measurement in very low permeability porous media," *Oil Gas Sci. Technol.-Revue d'IFP Energies Nouvelles* **67**, 387–401 (2012).
- Brace, W. F., Walsh, J. B., and Frangos, W. T., "Permeability of granite under high pressure," *J. Geophys. Res.* **73**, 2225–2236, <https://doi.org/10.1029/jb073i006p02225> (1968).
- Cheng, N.-S., Hao, Z., and Tan, S. K., "Comparison of quadratic and power law for nonlinear flow through porous media," *Exp. Therm. Fluid Sci.* **32**, 1538–1547 (2008).

- Darcy, H., *Les Fontaines Publiques de la ville de Dijon: Exposition et Application des Principes à Suivre et des Formules à Employer Dans les Questions de Distribution d'eau* (Victor Dalmont, 1856).
- Faulkner, D. R. and Rutter, E. H., "Comparisons of water and argon permeability in natural clay-bearing fault gouge under high pressure at 20°C," *J. Geophys. Res.: Solid Earth* **105**, 16415–16426, <https://doi.org/10.1029/2000jb900134> (2000).
- Fellah, Z. E. A., Fellah, M., Mitri, F. G., Sebaa, N., Depollier, C., and Lauriks, W., "Measuring permeability of porous materials at low frequency range via acoustic transmitted waves," *Rev. Sci. Instrum.* **78**, 114902 (2007).
- Fischer, G. J., "Chapter 8 the determination of permeability and storage capacity: Pore pressure oscillation method," *Int. Geophys.* **51**, 187–211 (1992).
- Gong, G., Zhao, G., Pang, W., Tian, M., Chen, B., Yang, M., and Song, Y., "Continuous measurement of gas permeability in non-homogeneous hydrate reservoirs under effective pressure via a novel apparatus," *Gas Sci. Eng.* **118**, 205091 (2023).
- Green, K. M., Hoff, W. D., Carter, M. A., Wilson, M. A., and Hyatt, J. P., "A high pressure permeameter for the measurement of liquid conductivity of porous construction materials," *Rev. Sci. Instrum.* **70**, 3397–3401 (1999).
- Hadia, N. J., Mitra, S. K., and Vinjamur, M., "Estimation of permeability heterogeneity in limestone outcrop by pressure measurements: Experiments and numerical simulation," *Exp. Therm. Fluid Sci.* **40**, 177–184 (2012).
- Hasanov, A. K., Prasad, M., and Batzle, M. L., "Simultaneous measurements of transport and poroelastic properties of rocks," *Rev. Sci. Instrum.* **88**, 124503 (2017).
- Hasanov, A. K., Dugan, B., and Batzle, M. L., "Numerical simulation of oscillating pore pressure experiments and inversion for permeability," *Water Resour. Res.* **56**, e2019WR025681, <https://doi.org/10.1029/2019wr025681> (2020).
- Jannot, Y., Degiovanni, A., Moyno, C., and Lasseux, D., "New developments of the Gas Research Institute method for the permeability measurement of porous media," *Rev. Sci. Instrum.* **92**, 065102 (2021).

- Jannot, Y. and Lasseux, D., "A new quasi-steady method to measure gas permeability of weakly permeable porous media," *Rev. Sci. Instrum.* **83**, 015113 (2012).
- Jannot, Y., Lasseux, D., Delottier, L., and Hamon, G., "A simultaneous determination of permeability and Klinkenberg coefficient from an unsteady-state pulse-decay experiment," in International Symposium of the Society of Core Analysts, Abu Dhabi, 2008.
- Jannot, Y., Lasseux, D., Vizé, G., and Hamon, G., "A detailed analysis of permeability and Klinkenberg coefficient estimation from unsteady-state pulse-decay or draw-down experiments," in International Symposium of the Society of Core Analysts, Calgary, Canada, 2007.
- Jin, G., Pérez, H. G., Al Dhamen, A. A., Ali, S. S., Nair, A., Agrawal, G., Khodja, M. R., Hussaini, S. R., Jangda, Z. Z., and Ali, A. Z., "Permeability measurement of organic-rich shale-comparison of various unsteady-state methods," in SPE Annual Technical Conference and Exhibition, 2015.
- Jones, C. and Meredith, P., "An experimental study of elastic wave propagation an isotropy and permeability an isotropy in an illitic shale," *Paper presented at the SPE/ISRM Rock Mechanics in Petroleum Engineering*, Norway, July 1998.
- Knabe, R. J. and Wang, Y., "Permeability characterization on tight gas samples using pore pressure oscillation method," *Petrophysics* **52**, 437–443 (2011).
- Kranz, R. L., Saltzman, J. S., and Blacic, J. D., "Hydraulic diffusivity measurements on laboratory rock samples using an oscillating pore pressure method," *Int. J. Rock Mech. Min. Sci. Geomech. Abstr.* **27**, 345–352 (1990).
- Lasseux, D., Jannot, Y., Profice, S., Mallet, M., and Hamon, G., "The 'Step Decay': A new transient method for the simultaneous determination of intrinsic permeability, Klinkenberg coefficient and porosity on very tight rocks," in International Symposium of the Society of Core Analysts, Aberdeen, Scotland, 2012.
- Lasseux, D., Parada, F. J. V., Tapia, J. A. O., and Goyeau, B., "A macroscopic model for slightly compressible gas slip-flow in homogeneous porous media," *Phys. Fluids* **26**, 053102 (2014).
- Lasseux, D., Valdés Parada, F. J., and Porter, M. L., "An improved macroscale model for gas slip flow in porous media," *J. Fluid Mech.* **805**, 118–146 (2016).
- Lasseux, D., Valdés-Parada, F. J., and Bellet, F., "Macroscopic model for unsteady flow in porous media," *J. Fluid Mech.* **862**, 283–311 (2019).
- Liu, J. F., Wu, W. T., Chiu, W. C., and Hsieh, W. H., "Measurement and correlation of friction characteristic of flow through foam matrixes," *Exp. Therm. Fluid Sci.* **30**, 329–336 (2006).
- Liu, G., Liu, J., Gao, F., and Zhang, G., "Constraints of pore-bulk strain ratio and interference time on the evolution of coal permeability during CO₂ injection," *Geofluids* **2021**, 6616315.
- Luffel, D. L. and Guidry, F. K., "New core analysis methods for measuring reservoir rock properties of devonian shale," *J. Pet. Technol.* **44**, 1184 (1992).
- Malkovsky, V. I., Zharikov, A. V., and Shmonov, V. M., "New methods for measuring the permeability of rock samples for a single-phase fluid," *Izvestiya, Phys. Solid Earth* **45**, 89–100 (2009).
- Metwally, Y. M. and Sondergeld, C. H., "Measuring low permeabilities of gas-sands and shales using a pressure transmission technique," *Int. J. Rock Mech. Min. Sci.* **48**, 1135–1144 (2011).
- Ohazuruike, L. and Lee, K. J., "A comprehensive review on clay swelling and illitization of smectite in natural subsurface formations and engineered barrier systems," *Nucl. Eng. Technol.* **55**, 1495–1506 (2023).
- Pamuk, M. T. and Özdemir, M., "Friction factor, permeability and inertial coefficient of oscillating flow through porous media of packed balls," *Exp. Therm. Fluid Sci.* **38**, 134–139 (2012).
- Sander, R., Pan, Z., and Connell, L. D., "Laboratory measurement of low permeability unconventional gas reservoir rocks: A review of experimental methods," *J. Nat. Gas Sci. Eng.* **37**, 248–279 (2017).
- Skjetne, E. and Auriault, J.-L., "Homogenization of wall-slip gas flow through porous media," *Transp. Porous Media* **36**, 293–306 (1999).
- Song, I. and Renner, J., "Experimental investigation into the scale dependence of fluid transport in heterogeneous rocks," *Pure Appl. Geophys.* **163**, 2103–2123 (2006).
- Tian, Z., Zhang, D., Wang, Y., Zhou, G., Zhang, S., and Wang, M., "Inertial solution for high-pressure-difference pulse-decay measurement through microporous media," *J. Fluid Mech.* **2023**, 971.
- Uehara, S.-i. and Shimamoto, T., "Gas permeability evolution of cataclaste and fault gouge in triaxial compression and implications for changes in fault-zone permeability structure through the earthquake cycle," *Tectonophysics* **378**, 183–195 (2004).
- Veltzke, T. and Thöming, J., "An analytically predictive model for moderately rarefied gas flow," *J. Fluid Mech.* **698**, 406–422 (2012).
- Wang, Z., Wang, M., and Chen, S., "Coupling of high Knudsen number and non-ideal gas effects in microporous media," *J. Fluid Mech.* **840**, 56–73 (2018).
- Wang, Y., Tian, Z., Nolte, S., Amann-Hildenbrand, A., Krooss, B. M., and Wang, M., "Reassessment of transient permeability measurement for tight rocks: The role of boundary and initial conditions," *J. Nat. Gas Sci. Eng.* **95**, 104173 (2021).
- Wang, Y., Tian, Z., Nolte, S., Krooss, B. M., and Wang, M., "An improved straight-line method for permeability and porosity determination for tight reservoirs using pulse-decay measurements," *J. Nat. Gas Sci. Eng.* **105**, 104708 (2022).
- Winhausen, L., Amann-Hildenbrand, A., Fink, R., Jalali, M., Khaledi, K., Hamdi, P., Urai, J. L., Schmatz, J., and Amann, F., "A comparative study on methods for determining the hydraulic properties of a clay shale," *Geophys. J. Int.* **224**, 1523–1539 (2020).
- Wyckoff, R. D., Botset, H. G., Muskat, M., and Reed, D. W., "The measurement of the permeability of porous media for homogeneous fluids," *Rev. Sci. Instrum.* **4**, 394–405 (1933).